

Adsorption of malachite green dye from solution by magnetic activated carbon in batch mode

Yachan Rong^a, Hui Li^a, Linghui Xiao^a, Qing Wang^a, Yanyan Hu^a, Shusheng Zhang^b, Runping Han^{a,*}

^aCollege of Chemistry and Molecular Engineering, ^bCenter of Modern Analysis and Computation, Zhengzhou University, No 100 Kexue Road, Zhengzhou, 450001 China, Tel. +86 371 67781757, Fax +86 371 67781556, email: 429052746@qq.com (Y. Rong), 15737156012@qq.com (H. Li), 1208854369@qq.com (L. Xiao), 565734174@qq.com (Q. Wang), 1793841545@qq.com (Y. Hu), zsszz@126.com (S. Zhang), rphan67@zzu.edu.cn (R. Han)

Received 3 November 2017; Accepted 17 February 2018

ABSTRACT

Magnetic activated carbon (MAC) was synthesized by co-precipitation method for the removal of cationic dye, malachite green (MG) from solution. The characterization of MAC was presented, such as Fourier transform infrared spectrum (FTIR), X-ray diffraction (XRD), thermogravimetric analysis (TGA) and BET surface area, etc. The results suggested that $\gamma\text{-Fe}_2\text{O}_3$ was the main magnetic phase. Adsorption studies were performed at a range of adsorbent dose, different pH, coexisted ions concentrations, contact time and dye concentration in the batch mode. Results showed that the value of pH at 8–9 was best for the adsorption and the adsorption capacity at 303 K could reach up to 766 $\text{mg}\cdot\text{g}^{-1}$. The equilibrium data were fitted well by Freundlich model while kinetic data were predicted by pseudo-first-order model. Thermodynamic parameters were calculated and the results showed that the process was spontaneous and endothermic in nature. In addition, MAC could be reused and the regeneration rate could reach up to 93.6% after three cycles. The results showed that MAC may be potential as a high-efficiency adsorbent for the removal of MG from aqueous solution.

Keywords: Adsorption; Magnetic activated carbon; Malachite green; Regeneration

1. Introduction

The environmental pollutions caused by dyes from various ways have drawn more attention in recent years [1,2]. As a result, various methods have been developed for removal of dyes from wastewater including adsorption, chemical and electrochemical oxidation, membrane separation process, photo degradation, etc [3–5]. Among these methods, adsorption technology is widely used as it is fast, easy-operated, effective and relatively inexpensive. Powder activated carbon with high surface area, pore volume, is widely used as an adsorbent in chemical and food industry [6] and be considered as one of the best material to remove contaminants in water or wastewater treatment process [7–9]. However, filtration or centrifugation as the

traditional method to separate powder activated carbon always had the drawback of blockage of filters and the loss of activated carbon [10]. Therefore, to make the full use of activated carbon and reduce the secondary pollution, it was important to find a quick and effective technique for separating activated carbon.

In recent years, the application of magnetic particles in adsorption has received considerable attention to solve environmental problems [11–13]. The magnetizations of adsorbents such as polypyrrole [14], polydopamine [15], polyaniline [16] coated magnetic particles and dipping [17] or doping [18] magnetic particles etc. were prepared for removal of dyes and other contaminants. Magnetic particles can be separated from the medium by a simple magnetic process. However, the uses of almost adsorbents have been limited because of their small adsorption capacity [19,20]. To solve this situation, different doping or co-precipitation methods using mag-

*Corresponding author.

netic particles and activated carbon were explored to purify water [17,21,22].

Malachite green (MG, cationic dye) was widely used in many industries for their coloring agent and it was discharged to water body during process of synthesis or use. MG is toxic and carcinogenic that can cause irritation, allergy and cancer in human [23–25]. Various adsorbents and photo catalysts were used to remove cationic dye from the wastewater [26–30]. Khattri and Singh studied the removal of MG from dye wastewater on neem sawdust and made the full use of Natural waste [31]. Malik et al. utilized groundnut shell waste to prepare powdered activated carbon as adsorbent and the adsorbent demonstrated attractive removal efficiency [32]. Yang et al. used oxygen-rich pentaerythritol to modify multi-walled carbon nano tube to remove alizarin yellow R and alizarin red S and showed strong adsorption capacity [33]. Yu et al. prepared TiO_2 -based photo catalysts to degrade methylene blue, rhodamine B and methyl orange and also realized the aim of water purification [34]. In this paper, the magnetic activated carbon which was prepared by ferric salts and activated carbon through co-precipitation method had not been used for removal the MG in the wastewater. So the cationic dye pollutant, MG, was chosen as objective pollutant.

In this study, magnetic activated carbon (MAC) was prepared by co-precipitation for fast and effective removal of MG from solution. Several characterizations of MAC were presented and its property of adsorption toward MG was performed. Moreover, the equilibrium and kinetics data were analyzed and thermodynamic parameters were calculated. Regeneration and reuse of MG-loaded MAC were also performed.

2. Material and methods

2.1. Materials

Ferric Chloride (FeCl_3 , Fengchuan Chemical Reagent, Tianjin, China), ferrous sulfate (FeSO_4 , Sinopharm Chemical Reagent, Shanghai, China), ammonium hydroxide (25%–28%, w/w, Sinopharm Chemical Reagent, Shanghai, China), Sodium chloride (NaCl , Kermel, Tianjin, China), Calcium chloride (CaCl_2 , Kermel, Tianjin, China), cetyltrimethyl ammonium bromide (CTAB, Sinopharm Chemical Reagent, Shanghai, China), Absolute ethanol (Fuchen Chemical Reagent, Tianjin, China), Polyethylene glycol-6000 (Sinopharm Chemical Reagent, Shanghai, China), Activated charcoal (Macklin, Shanghai, China). Malachite green dye (Kermel, China) was purchased from Tianjin, China and its structure was shown in Fig. 1. All chemicals were of analytical grade and used without further purification. Distilled water was used.

2.2. Preparation of magnetic activated carbon (MAC) and magnetic particle (MP)

The magnetic activated carbon was prepared by co-precipitation. 1.6 g of activated carbon and 0.04 g of polyethylene glycol-6000 were placed in beaker and dissolved in distilled water with mechanical agitation (15 min). Subse-

quently 2.03 g of FeCl_3 and 1.39 g of FeSO_4 were added while stirring for 30 min. Ammonia solution (pH = 12.5) was added drop wise until the pH value of the solution reach up to 11. After the reaction, the solution was aged for 30 min. The whole process was carried out at 50°C (water-bath). Magnetically modified activated carbon was collected by magnet and then washed by water till the pH of supernatant was approximately 7. Then it was placed in oven at 60°C to drying. Magnetic particle (MP) was prepared by the same method without activated carbon [21].

2.3. Characterization of MAC and MP

The determination of pH_{pzc} was conducted by adjusting pH of 10 ml 0.01 mol·L⁻¹ NaCl solution to a value between 2 and 12 in 50 ml flasks. 0.010 g MAC was added in solution and equilibrium time was 90 min. Then pH_{final} of solution was measured by pH meter. The pH_{pzc} is the point where $\text{pH}_{\text{initial}} - \text{pH}_{\text{final}} = 0$.

The Fourier transform infrared (FTIR) spectroscopy (FTIR-2000, PerkinElmer) was measured to determinate characteristic functional groups of MP, MAC and MAC-MG (MG adsorbed MAC). It aimed to demonstrate the successful of co-precipitation of AC and MP and the adsorption of MG onto MAC.

Boehm titration was used to determine the amount of surface acidic and basic functional groups. Each sample (0.400 g) was accurately weighed and shook with 0.05 mol·L⁻¹ HCl, NaOH, Na_2CO_3 , NaHCO_3 in a closed flask and agitated for 24 h at room temperature. After the reaction, the remaining HCl, NaOH, Na_2CO_3 , NaHCO_3 were determined by titration using 0.05 mol·L⁻¹ NaOH or HCl, respectively [35].

X-ray diffraction (XRD) analysis was used to identify any crystallographic structure in MAC using a computer-controlled X-ray diffractometer (X' Pert PRO, China).

Thermogravimetric (TGA) analysis was performed to quantify the content of AC in MAC using Simultaneous Thermal Analyzer (STA 409 PC, Germany). MP and MAC was heated from 303 K to 873 K at 3 K·min⁻¹, under air atmosphere, respectively.

Scanning electron microscopy (SEM) was a technique to observe the micro morphology of the material. In

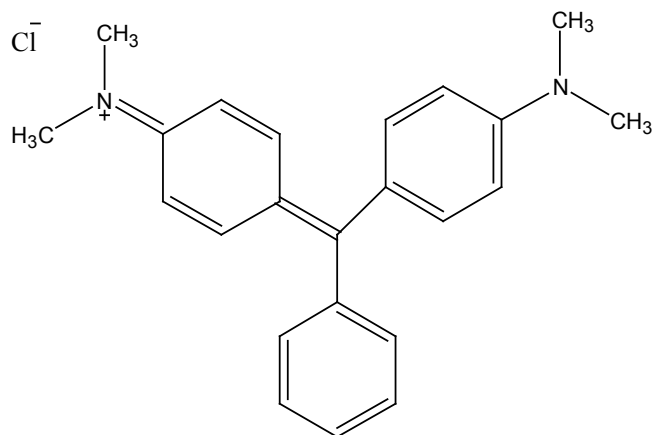


Fig. 1. The structure of MG.

this paper, the micro morphology of MP and MAC was observed under 15.0 kV with scanning electron microscope (Su8020, China).

The Brunauer–Emmett–Teller (BET) method was used to measure the specific surface area of MAC by an Automated Gas Sorption Analyzer (Autosorb-iQ, China). The precisely weighed MAC (0.1529 g) was degassed at 100° and adsorbed under N₂ at 77 K.

UV-vis spectroscopic measurements were carried out to determine the concentrations of MG left in supernatant solutions referring to the standard curve of MG at the maximum wavelength (615 nm) (UV/VIS-3000, China).

2.4. Adsorption experiments

Batch adsorption experiments with 10 ml of MG solution in 50 mL conical flasks were performed for various dose (1–22 mg, $C_{MG} = 800 \text{ mg}\cdot\text{L}^{-1}$), 5 to 720 min contact times ($C_{MG} = 400 \text{ mg}\cdot\text{L}^{-1}$), coexisted ions (NaCl, CaCl₂, CTAB), 3–9 pH ($C_{MG} = 400 \text{ mg}\cdot\text{L}^{-1}$) and 20, 25 and 30°C ($C_{MG} = 300\text{--}1000 \text{ mg}\cdot\text{L}^{-1}$, pH = 8–9). Then the conical flasks were placed and shook in an orbital shaker (SHZ-82, China) at 120 rpm. Solution pH was adjusted by 1.0 mol·L⁻¹ of hydrochloric acid and sodium hydroxide solutions and the pH values of MG solutions were measured by a pH meter (PHS-3C, China). After adsorption, the samples were withdrawn from the flasks by magnet. The concentration of MG in the supernatant solution was analyzed by measuring the absorbance at 615 nm.

The data obtained in batch mode studies were used to calculate the MG uptake quantity. The quantity of MG adsorbed onto unit weight of adsorbent (q_t or q_e , mg·g⁻¹) and the dye removal efficiency (p , %) were calculated using the following equations, respectively:

$$q = \frac{V(C_0 - C)}{m} \quad (1)$$

$$p = \frac{(C_0 - C_e)}{C_0} \times 100\% \quad (2)$$

where C_0 is the initial MG concentration (mg·L⁻¹), C_t or C_e is the MG concentration at any time t or equilibrium (mg·L⁻¹), V is the reaction solution volume (L), and m is the mass of MAC (g).

To investigate the reusability of MAC, the regeneration and re-adsorption of MG experiments were conducted. Several methods of regeneration were chosen and three continuous circulations were carried out. Each cycle consists of adsorption ($t = 360 \text{ min}$, pH = 9, MAC dose = 0.5 g·L⁻¹, $C_0 = 400 \text{ mg}\cdot\text{L}^{-1}$, $T = 303\text{K}$) followed by desorption ($t = 360 \text{ min}$). After adsorption reaction, the resultant MG-loaded MAC (MG-MAC) was collected, washed and air dried and reintroduced into the desorption experiments. The desorption efficiency and regeneration efficiency were calculated in the following:

$$D = \frac{m}{m_c} \times 100\% \quad (3)$$

$$\eta = \frac{q_n}{q_e} \times 100\% \quad (4)$$

where D is the desorption efficiency of the adsorbent (%); m is the MG mass (g), which is desorbed from the adsorbent and m_c is the remaining MG mass on the adsorbent before desorption (g). η is regeneration efficiency of the adsorbent (%), q_n and q_e are the adsorption quantity of regenerative MAC for n (1, 2, 3) times and the fresh MAC in the same experimental conditions, respectively.

3. Results and discussion

3.1. Characterization of MAC and MP

3.1.1. FTIR analysis

FTIR of MP, MAC and MG-MAC are presented in Fig. 2. They all showed the similar infrared adsorption between 500 and 700 cm⁻¹. The wide peak around 3400 cm⁻¹ of MAC and MP represented the –OH stretching vibrations due to activated carbon. The peaks between 1650 cm⁻¹ and 1450 cm⁻¹ belonged to the benzene ring. At fingerprint region, the small peak near 886 cm⁻¹ could be assigned to C–H bending vibration. The characteristic peak of iron oxides was located at 587 cm⁻¹ [36,37]. From Fig. 2, strong peak located at 3300 cm⁻¹ about MG-loaded MAC was due to stretching vibration of –OH from adsorbed water. The peak located at 1620 cm⁻¹ from benzene ring framework was obvious seen as there was benzene ring in MG molecular. Absorption peak near 1375 cm⁻¹ was due to bending vibration of –CH₃ from MG structure. Peak from iron oxides was still observed at 587 cm⁻¹. These confirmed that MG was adsorbed onto surface of MAC.

3.1.2. Zero point of charge

The zero point of charge of materials indicated the functional groups on their surface and the results are shown in Fig. 3. It is seen from Fig. 3 that the pH_{pzc} values are nearly 7.1 for both two materials. This illustrated that the amount of charge on the surface of MP and MAC was no change.

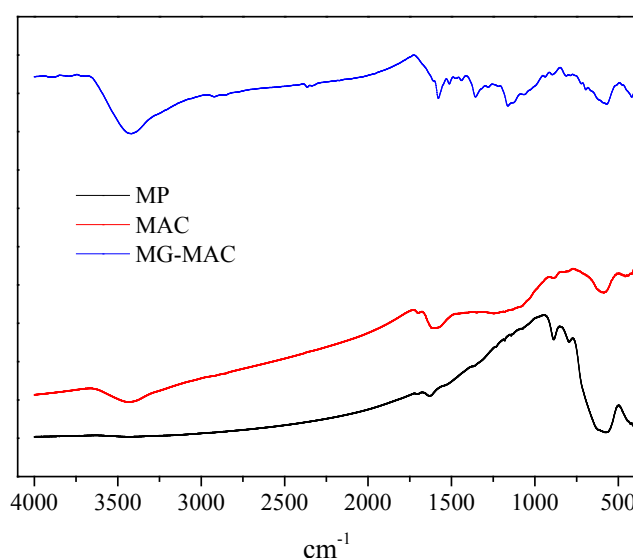


Fig. 2. FTIR of MP, MAC and MG-loaded MAC.

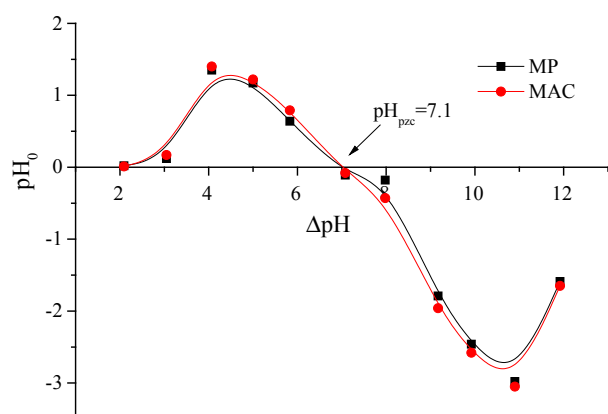


Fig. 3. Plots of ΔpH against initial pH for the determination of pH_{pzc} of MAC and MP.

3.1.3. Boehm titration

The number of acidic and basic functional groups of MP and MAC are listed in Table 1. The iron oxides in MAC reacted with hydrochloric acid and could not obtain the amount of basic functional groups on its surface. In Table 1 there are more acidic groups for AC and less basic groups. Furthermore, there are more carboxyl and phenolic groups and less lactonic groups. For MAC, there are comparatively less acidic groups. It was also found that there were much more phenolic groups and less carboxyl and lactonic groups for MAC.

3.1.4. XRD analysis

The XRD patterns of MP and MAC are presented in Fig. 4. The analysis results suggested that the peaks may relate to the presence of $\gamma\text{-Fe}_2\text{O}_3$ or Fe_3O_4 . Maybe one or two iron oxide existed in MP and MAC. In addition, the boarder peaks for MAC indicated a smaller crystallite size than MP according to Scherrer's equation [38].

3.1.5. TGA analysis

Thermogravimetric analysis of MP and MAC are shown in Fig. 5. No weight gain was observed during the course of continuous heating, indicating that no Fe^{2+} was oxidized to Fe^{3+} . Combining the appearance and magnetic characteristics of magnetic particles, it was presumed that the magnetic particles were $\gamma\text{-Fe}_2\text{O}_3$. For MP analysis, the weight loss was observed. It could be attributed to water vapor ($<200^\circ\text{C}$) and the oxidation of dispersant (glycol) which was introduced in the preparation of materials ($<200^\circ\text{C}$). MAC showed weight loss of 6.22% due to water at the temperature lower 200°C . In the temperature range $200\text{--}600^\circ\text{C}$, weight loss of 54.84% was related to the oxidation of carbon [39]. Based on the analysis results, it was estimated that the mass fraction of AC in MAC was about 50%.

3.1.6. SEM analysis

Fig. 6 shows the scanning electron microscopy of MP and MAC. From Fig. 6, the particles of MP and MAC are

Table 1
Quantity of surface acidic and basic functional groups of MAC and MP

	AC	MAC
Surface basicity ($\text{mmol}\cdot\text{g}^{-1}$)	0.0528	–
Surface acidity ($\text{mmol}\cdot\text{g}^{-1}$)	0.388	0.335
Carboxyl ($\text{mmol}\cdot\text{g}^{-1}$)	0.164	0.0178
Lactonic ($\text{mmol}\cdot\text{g}^{-1}$)	0.0641	0.0743
Phenolic ($\text{mmol}\cdot\text{g}^{-1}$)	0.163	0.243

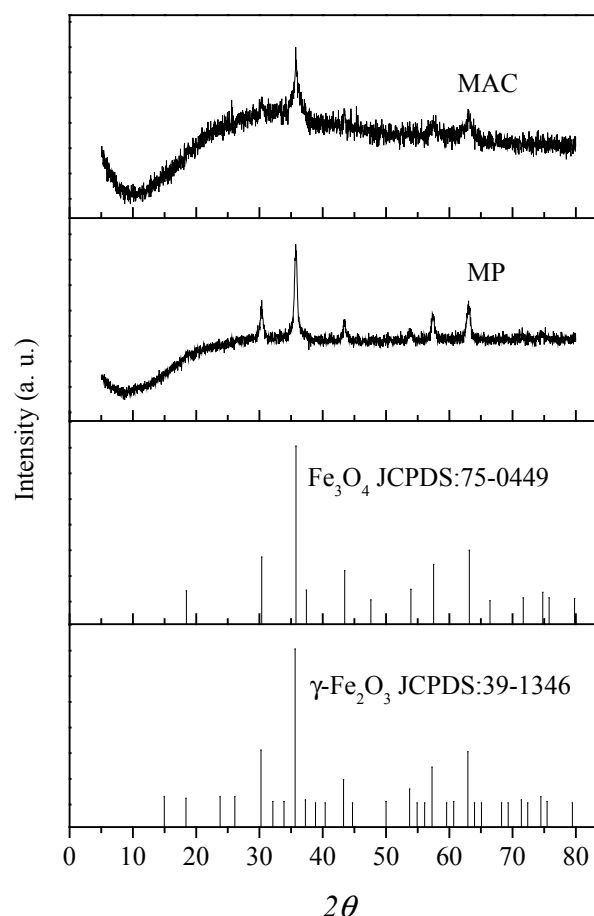


Fig. 4. XRD pattern of MP and MAC.

not uniform and the size of more particles is less than $1\ \mu\text{m}$. Some particles were aggregated. It was also seen that MAC and MP exhibited granular micro structure with irregular shaped grains [36,37].

3.1.6. The BET surface area

The adsorption isotherm of N_2 on MAC is illustrated in Fig. 7. The Brunauer Emmette Teller method (BET, the most usual standard procedure) was used to calculate the surface area and it was $1130\ \text{m}^2\cdot\text{g}^{-1}$. The results suggested that the MAC may be promise to be as a superior adsorbent.

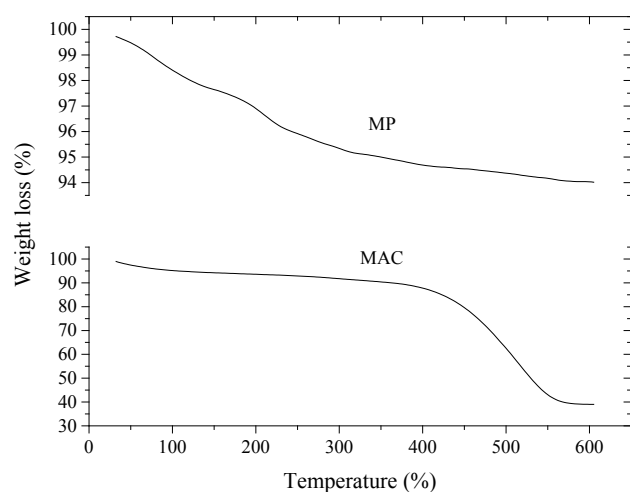


Fig. 5. Thermogravimetric analysis of MP and MAC.

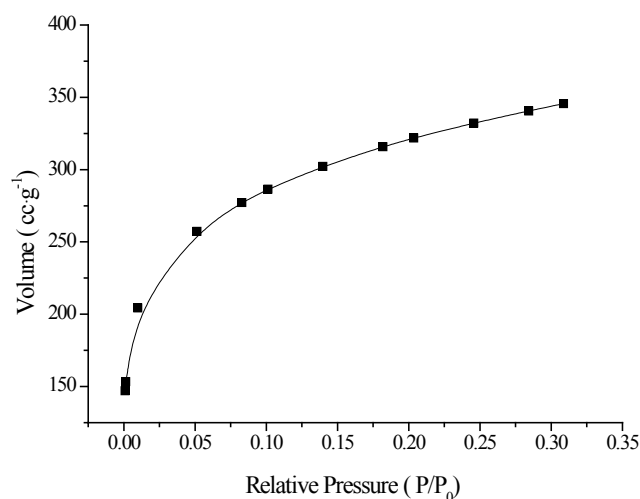


Fig. 7. Nitrogen adsorption isotherm of MAC.

It was concluded from analysis of characterization that MAC was favor of adsorption as there was higher surface area and irregular shaped forms, besides its easy separation from solution through external magnet.

3.2. Adsorption study

3.2.1. Effect of adsorbent dosage on adsorption quantity

The determination of optimum dosage of adsorbent is dispensable and its effect is shown in Fig. 8. It is seen from Fig. 8 that the values of q_e decreased and the removal efficiency (p) values increased gradually with the increase of adsorbent dosage. It was inferred that the active sites increased along with the adsorbent dosage increased. As can be seen in Fig. 8 that the two values of q_e and p are in the medium level when the adsorbent dosage is $0.5 \text{ g}\cdot\text{L}^{-1}$ and it was chosen as the option dosage in next test.

3.2.2. Effect of contact time on adsorption quantity

The effect of contact time on the adsorption process is demonstrated in Fig. 9. The adsorption process contained three parts: first 5–70 min was the initial phase of rapid adsorption and then 70–150 min was a slow process until equilibrium at 240 min. The results might be attributed to much more active sites and stronger driving force in the early stage of adsorption and the slow adsorption rate at the end due to the saturation of binding sites [40,41]. The whole adsorption process reached equilibrium quickly, essentially due to the large specific surface area and rich pore structure. The equilibrium time was taken as 360 min for further experiments. In addition, the comparison of MP and MAC toward MG showed that MAC had large adsorption quantity and MAC was a promising adsorbent to remove MG from solution.

3.2.3. Effect of coexisted ions on adsorption quantity

The effect of coexisting ions should also be considered in the wastewater treatment. Considering that the mal-

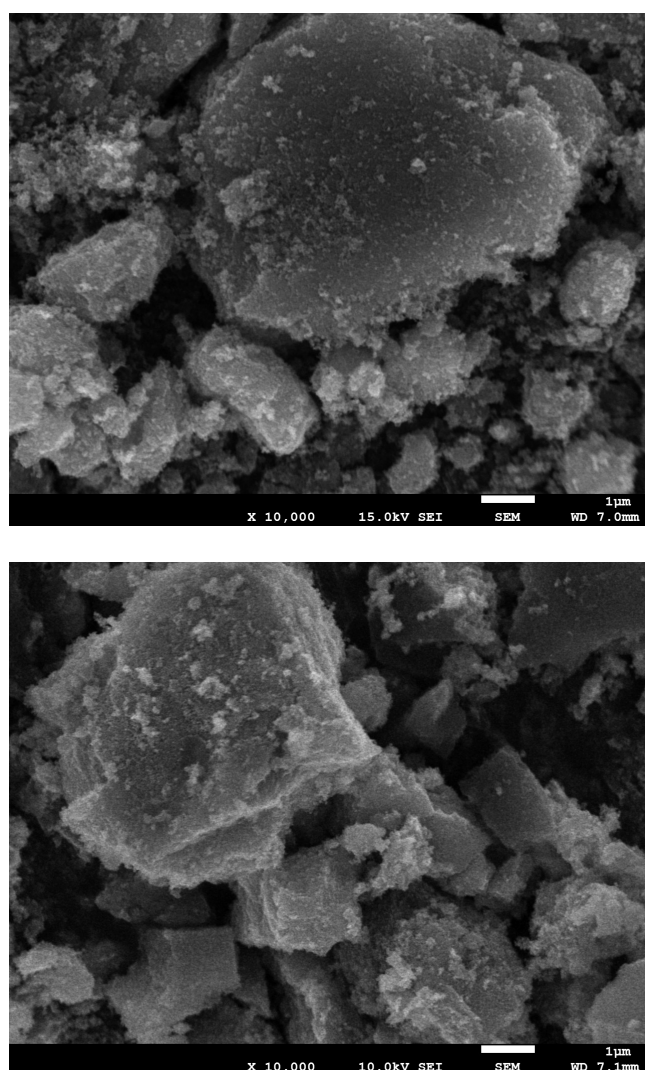


Fig. 6. SEM analysis (a) MP; (b) MAC.

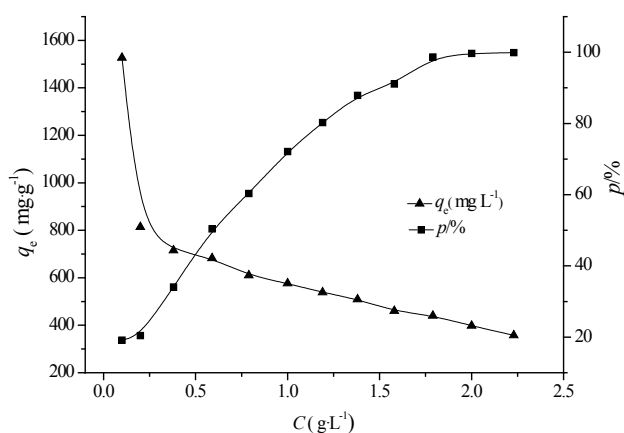


Fig. 8. Effect of adsorbent dose on adsorption quantity.

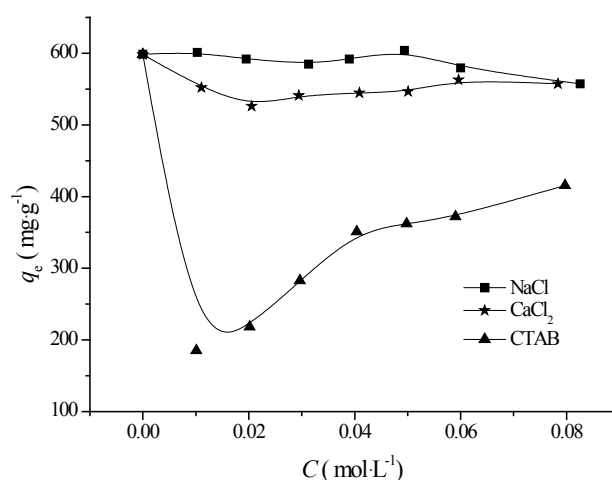


Fig. 10. Effect of coexisted ions on adsorption quantity.

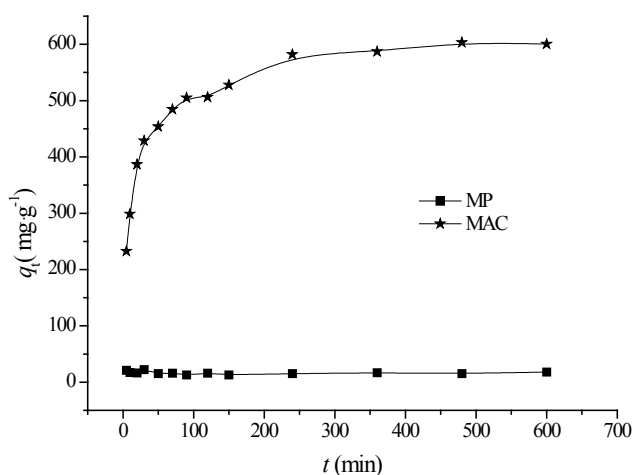


Fig. 9. Effect of contact time on adsorption quantity of MP and MAC.

achite green was a cationic dye and contained the hydrophilic element (N), NaCl, CaCl₂ and CTAB were selected as the coexisting ion. Fig. 10 shows the effects of different concentrations of NaCl, CaCl₂ and CTAB on the values of q_e . As can be seen from Fig. 10 that the presence of NaCl and CaCl₂ had slightly negative effect on the values of q_e . It suggested that electrostatic attraction existed in the adsorption process but not the dominant force [42]. In addition, the existence of CTAB negatively affected the values of q_e and the negative effects decreased as the concentration of CTAB was increased. The critical micelle concentration of CTAB at 308 K was $9.2 \times 10^{-4} \text{ mol} \cdot \text{L}^{-1}$. It was conferred that the micelle of CTAB formed and the force of CTAB with MAC was weakened. The negative effect of CTAB for adsorption process inferred that the hydrophilic group of CTAB, not MG, also combined with the oxygen-containing functional groups of MAC by hydrogen bond [43].

3.2.3. Effect of pH on adsorption quantity

To study the effect of pH on the adsorption, the initial pH was adjusted within 3–9 and the results are presented in

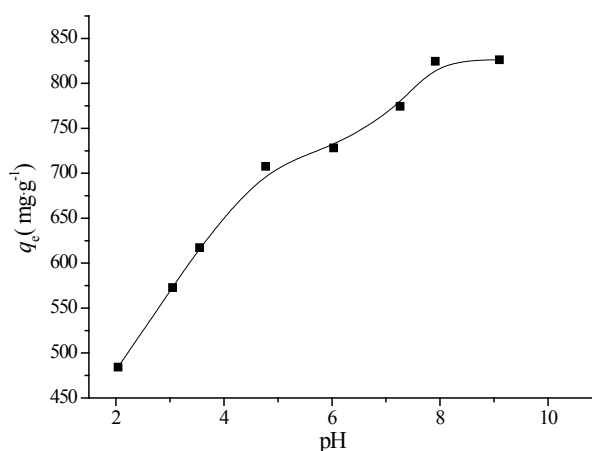


Fig. 11. Effect of pH on adsorption quantity.

Fig. 11. The values of q_e became larger with the increase of pH from 2 to 8. When the value of pH was over 8, the adsorption capacity changed little and the pH of the working solution was adjusted to 8–9. As pH_{pzc} of MAC was 7.1 and MG was cationic dye, MG was easily adsorbed on MAC surface at alkaline conditions through electrostatic attraction. Also, at acidic solution, the presence of excess H⁺ competed with MG adsorbed on MAC [44,45]. From Fig. 10, even at pH = 2, there was still some adsorption quantity compared to pH = 8. This showed that there were other actions between MAC and MG, such as π - π dispersion, hydrogen-bonding, etc [6].

3.2.4. The effect of MG concentration and temperature on adsorption quantity

The initial concentration and adsorption temperature influence much on the adsorption process [46]. The effectiveness of equilibrium MG concentration and temperature are researched and the results are shown in Fig. 12. It can be seen that the value of q_e increased with the increase of MG

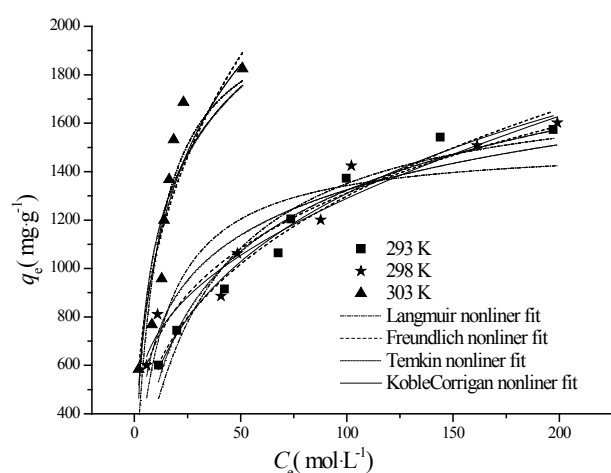


Fig. 12. Adsorption isotherms of MG adsorption onto MAC at various temperatures.

concentration. This could be attributed to the driving force of the concentration gradient.

In Fig. 12, when the temperature was 303 K, the adsorption capacity was better than 293 K and 298 K while the adsorption capacity was nearly equal at $T = 293, 298$ K. The results indicated that the adsorption process was endothermic and insensitive to temperature at lower temperature. The experimental data showed that the maximum adsorption capacity was up to $1830 \text{ mg}\cdot\text{g}^{-1}$. The comparison of MG adsorption capacity by MAC and other adsorbents is listed in Table 2. It can be referred that MAC have superior capacity for MG from solution.

3.3. Isotherm studies

In order to figure out the adsorption mechanism of MG on MAC, the Langmuir, Freundlich, Temkin models were used to fit the adsorption isotherm. The used models are listed in Table 3. The fitting parameters and the determined coefficients (R^2) are listed in Table 4 by nonlinear regressive analysis and the fitted curves are also shown in Fig. 12.

In Table 4 there are higher values of R^2 for Freundlich model. Freundlich model is an empirical formula used to describe the adsorption process of high concentration adsorbates on heterogeneous surfaces. The adsorption coefficient K_F increased with the increase of temperature, which indicated that the increase of temperature was beneficial to the adsorption process. The fitting parameters $1/n$ was between 0 and 0.5, illustrating easily adsorption.

3.4. Kinetic studies

In order to explore the mechanism of MG on adsorbent and figure out what controls the process, kinetic analysis were performed. The experimental data were fitted by three models, namely pseudo-first-order kinetic model, pseudo-second-order kinetic model and Elovich equation (equations also presented in Table 3).

Table 2

Comparison of monolayer adsorption capacity of MG onto various adsorbents

Adsorbent	q_m ($\text{mg}\cdot\text{g}^{-1}$)	Reference
MAC	2138	This study
Almond gum	196.07	[1]
Activated carbon/ $\text{Co}_2\text{Fe}_2\text{O}_4$ composites	89.29	[10]
Magnetic activated carbon (impregnation)	333	[17]
Cellulose aerogel	212.7	[23]
Bagasse fly ash	170.33	[45]
β -cyclodextrin-graphene oxide nano composites	990.10	[47]
CO_2 -activated porous carbon	295.86	[48]
Magnetic barium phosphate composite	1639	[49]
Jute fiber carbon	136.58	[50]
Iron nano particles loaded on ash	500.0	[51]
Reduced graphene oxide	476.2	[52]
Aminopropyl functionalized magnesium phyllosilicate	334.80	[53]
Natural zeolite	273	[54]
Rambutan peel-based activated carbon	418.60	[55]

The fitting result was evaluated by R^2 and all the obtained parameters are listed in Table 5. The experimental and fitted curves were compared and are illustrated in Fig. 13. As shown in Table 5, all the adsorption rate constant values (k_1, k_2, α) which were obtained from the fitting results increased with the increase of adsorption temperature. It suggested that the increase of temperature was beneficial to raise the reaction rate [56]. Furthermore, the $q_{e(\text{exp})}$ values also increased with the increase of temperature and this showed that the adsorption process was an endothermic process, which was in accordance with the results of the isotherm studies. In addition, comparing the R^2 values of three fitting models and the degree of proximity between $q_{e(\text{exp})}$ and $q_{e(\text{theo})}$ from pseudo-first-order kinetic model and pseudo-second-order kinetic model, it was found that pseudo-first-order kinetic model was best to describe the adsorption process. Therefore, it was confirmed that the MG over MAC was controlled by physisorption process [49].

3.5. Thermodynamic studies

Temperature change had effect on MG adsorption. The temperature dependence of adsorption is related to various thermodynamics parameters. The thermodynamics parameters, including Gibbs free energy (ΔG_0), enthalpy (ΔH_0), entropy (ΔS_0) and activation energy (Ea) were calculated by the following formula [6].

Table 3
Adsorption equilibrium models: description and nomenclature

Models	Non linear form	Nomenclature
Isotherm model		
Langmuir	$q_e = \frac{q_m K_L C_e}{1 + K_L C_e}$	q_m (mg·g ⁻¹) = mono layer maximum adsorption quantity; K_L (L·mg ⁻¹) = Langmuir constant related to binding energy.
Freundlich	$q_e = K_F C_e^{1/n}$	K_F (L·g ⁻¹) and n are Freundlich constant depending on temperature.
Koble-Corrigan	$q_e = \frac{A C_e^n}{1 + B C_e^n}$	A (L·mg ⁻¹) and B (L·mg ⁻¹) are related to the capacity of adsorption.
Temkin	$q_e = A + B \ln C_e$	A and B (J·mg ⁻¹) are Temkin constants.
Kinetic model		
Pseudo-first-order kinetic	$q_t = q_e(1 - e^{-k_1 t})$	k_1 (min ⁻¹) is the rate constant, q_e (mg·g ⁻¹) or q_t (mg·g ⁻¹) is the amount of solute adsorbed on adsorbent at equilibrium or any time t .
Pseudo-second-order kinetic	$q_t = \frac{k_2 q_e^2 t}{1 + k_2 q_e t}$	k_2 (mg·g ⁻¹ ·min ⁻¹) is the rate constant.
Elovich	$q_t = \frac{1}{\beta} \ln(\alpha\beta) + \frac{1}{\beta} \ln t$	α (mg g ⁻¹ min ⁻¹): initial sorption rate constant, β (g mg ⁻¹): desorption constant.

Table 4
The parameters of isotherms at different temperatures by nonlinear regressive analysis

Langmuir				
T/K	K_L (L·g ⁻¹)	$q_{e(\text{exp})}$ (mg·g ⁻¹)	$q_{m(\text{theo})}$ (mg·g ⁻¹)	R^2
293	0.0306	1.57×10 ³	1.79×10 ³	0.918
298	0.0708	1.60×10 ³	1.52×10 ³	0.751
303	0.0926	1.83×10 ³	2.14×10 ³	0.672
Freundlich				
T/K	K_F	1/n	R^2	
293	257	0.352	0.970	
298	366	0.277	0.935	
303	454	0.363	0.698	
Temkin				
T/K	A	B	R^2	
293	-353	364	0.952	
298	83.4	270	0.887	
303	182	401	0.678	
Koble-Corrigan				
T/K	A	B	n	R^2
293	218	0.0432	0.455	0.966
298	259	-0.435	0.0983	0.932
303	405	0.105	0.554	0.646

Table 5
Parameters of kinetic analysis by pseudo-first-order and pseudo-second-order models

Pseudo-first-order equation				
T/K	$q_{e(\text{exp})}$ (mg·g ⁻¹)	$q_{e(\text{theo})}$ (mg·g ⁻¹)	k_1 (min ⁻¹)	R^2
293	695	659	0.0349	0.967
303	766	733	0.0600	0.981
313	811	790	0.0706	0.994
Pseudo-second-order equation				
T/K	$q_{e(\text{exp})}$ (mg·g ⁻¹)	$q_{e(\text{theo})}$ (mg·g ⁻¹)	k_2 (g·mg ⁻¹ ·min ⁻¹)	R^2
293	695	765	5.57×10 ⁻⁵	0.994
303	766	825	9.29×10 ⁻⁵	0.974
313	811	880	1.08×10 ⁻⁴	0.958
Elovich equation				
T/K	α (mg·g ⁻¹ ·min ⁻¹)	β (g·mg ⁻¹)	R^2	
293	80.8	0.00661	0.983	
303	176.1	0.006645	0.891	
313	282.4	0.00668	0.821	

$$K'_c = \frac{C_{\text{ad},e}}{C_e} \quad (7)$$

where K'_c is apparent adsorption equilibrium constant. $C_{\text{ad},e}$ represents the equilibrium concentration of MG on the adsorbent. K'_c is calculated at lowest experimental concen-

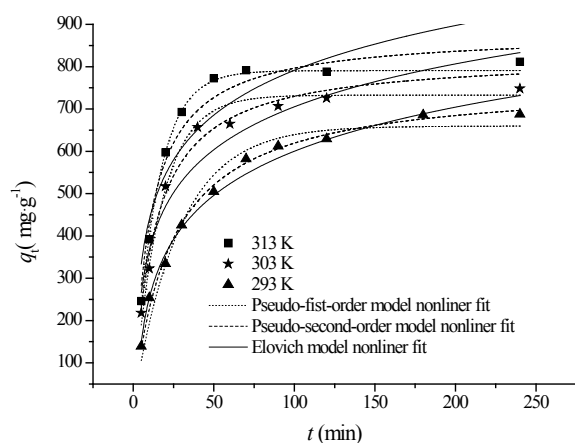


Fig. 13. Effect of contact time on adsorption quantity and kinetic model fitted curves.

tration, as K_c' needs to be obtained at very dilute concentration in theory. The ΔG_0 (Gibbs free energy) value is obtained by K_c' , based on the following formula.

$$\Delta G^0 = -RT \ln K_c' \quad (8)$$

where T is the experimental temperature (K) and R is universal gas constant ($8.314 \text{ J}\cdot\text{mol}^{-1}\cdot\text{K}^{-1}$). The ΔH^0 and ΔS^0 value are obtained by intercept and slope of Van't Hoff plot in the basis of the liner relationship between ΔG^0 and T .

$$\Delta G^0 = \Delta H^0 - T\Delta S^{0e} \quad (9)$$

The activation energy (E_a) is defined as the minimum energy barrier required for the combination of MG and MAC. The value of E_a was obtained by linear relation between $\ln k_1$ and $1/T$ in the general Arrhenius equation. The Arrhenius equation was given as follows:

$$\ln k_1 = -\frac{E_a}{RT} + \ln A \quad (10)$$

where k_1 is the rate constant and A (min^{-1}) is pre-exponential factor.

Thermodynamic parameters are listed in Table 6 according to Eqs. (8)–(10). The negative values of ΔG^0 at various temperatures showed the spontaneity of the MG adsorption process, confirming the affinity of MAC for MG. The increment in the absolute of ΔG^0 with the increase in temperature indicated the adsorption process favored at higher temperature. Usually, a value of ΔG^0 between 0 and $-20 \text{ kJ}\cdot\text{mol}^{-1}$ is consistent with electrostatic interaction between adsorption sites and the adsorbing ion, while ΔG^0 values more negative than $40 \text{ kJ}\cdot\text{mol}^{-1}$ involve charge sharing or transfer from surface of adsorbent to adsorbate to form a coordinate bond [57]. As shown in Table 6, the magnitude of ΔG^0 for this adsorption system is within the physical adsorption range.

Table 6
Thermodynamic parameters of MG adsorption

E_a ($\text{kJ}\cdot\text{mol}^{-1}$)	ΔH^0 ($\text{kJ}\cdot\text{mol}^{-1}$)	ΔS^0 ($\text{J}\cdot\text{mol}^{-1}\cdot\text{K}^{-1}$)	ΔG^0 ($\text{kJ}\cdot\text{mol}^{-1}$)		
			293 K	303 K	313 K
27.0	55.5	216	-7.88	-9.58	-12.2

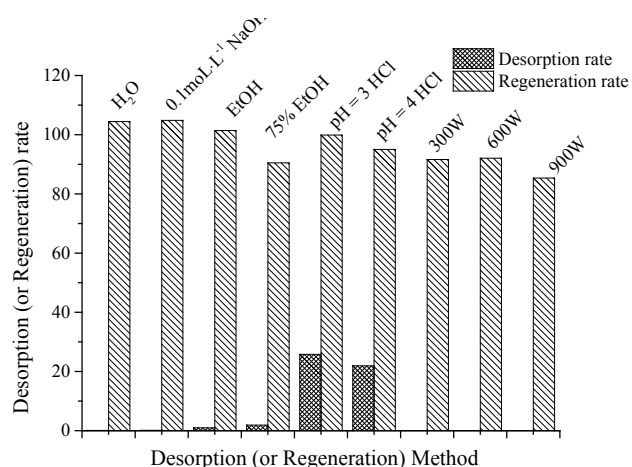


Fig. 14. Desorption rate and regeneration rate of different desorption methods.

The positive values of ΔH^0 showed that the process was endothermic, while the positive value of ΔS^0 ($216 \text{ J}\cdot\text{mol}^{-1}\cdot\text{K}^{-1}$) indicated an increase in the degree of freedom (or disorder) of the adsorbed species. The low value of E_a agreed well with the kinetic fitting results, indicating that the adsorption process was physical adsorption. All these thermodynamic parameters illustrated that MAC had a good adsorption capacity.

3.6. Regeneration of the adsorbent

Regeneration of used adsorbent and possible recovery of adsorbate will make the adsorption process economical [58–61].

In order to explore the availability of adsorbent, the reusability of MAC was studied. Various methods were used for desorption and regeneration study and the results are shown in Fig. 14. From Fig. 14, almost all of the methods used for desorption had no desorption efficiency except using HCl solution as desorption agent. It could be conferred that H^+ replace the position of MG on MAC and may be attributed to the existence of ion exchange during desorption process. Furthermore, It could also be seen that all materials possessed high regeneration efficiency (all above 85.4%) and probably because the adsorption was not saturated at first time. Three methods were chosen as the eluent for three times circulation. The results in Fig. 15 shows that the desorption rate of HCl solution gradually decreased, regardless of the concentration, while the distilled water had almost no desorption rate. It could also be found that the greater the concentration of H^+ , the better the desorption effect. The regeneration results are shown in Fig.

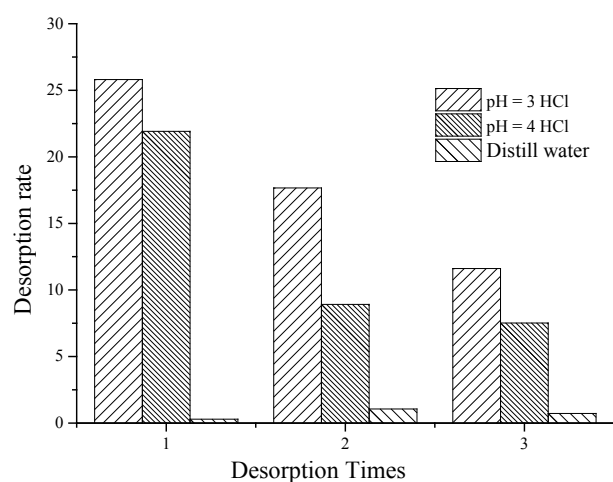


Fig. 15. Desorption rate of three cycles using pH = 3 HCl, pH = 4 HCl, distill water as desorption solution, respectively.

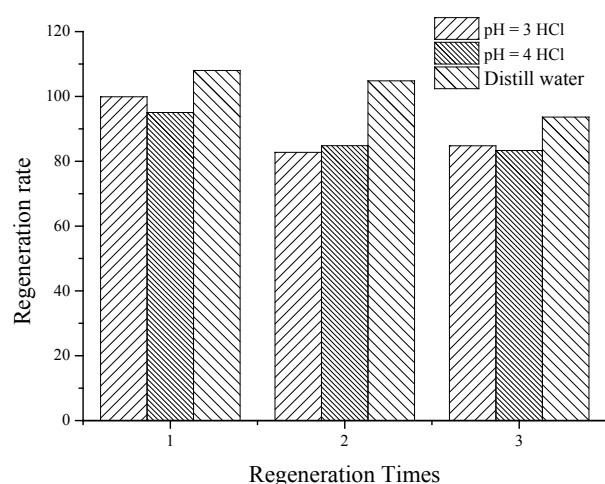


Fig. 16. Regeneration rate of three cycles after using pH = 3 HCl, pH = 4 HCl, distill water as desorption solution.

16. The regeneration capacity of HCl solution treated adsorbent was weaker than that of distill water treated. It was presumed that the positive charge of adsorbent increased with the treatment of H^+ , but the regeneration ability was still strong after three cycles.

4. Conclusion

In this work, the adsorption of MG on MAC was studied. The optimum conditions were established as $0.5 \text{ g}\cdot\text{L}^{-1}$ adsorbent dosage, 360 min as contact time and pH of 8–9. There was still some adsorption capacity under acidic conditions, indicating the adsorption process was not purely electrostatic attraction but π - π disperse. The co-existed CTAB had negative effect on adsorption, suggesting the existence of hydrogen bonding forces during adsorption process. The experimental data were well described by Freundlich model and Pseudo-first-order kinetic model

and the activation energy value was $27.0 \text{ kJ}\cdot\text{mol}^{-1}$, which indicated that the adsorption was multilayer and physical adsorption process. The adsorption was spontaneous and endothermic. Furthermore, MAC had strong regeneration capacity. Based on all this, MAC can be used as an excellent adsorbent to remove MG from solution.

Reference

- [1] F. Bouaziz, M. Koubaa, F. Kallel, R.E. Ghorbel, S.E. Chaabouni, Adsorptive removal of malachite green from aqueous solutions by almond gum: Kinetic study and equilibrium isotherms, *Int. J. Biol. Macromol.*, DOI <http://dx.doi.org/10.1016/j.ijbiomac.2017.06.106> (2017).
- [2] S. Srivastava, R. Sinha, D. Roy, Toxicological effects of malachite green, *Aquat. Toxicol.*, 66 (2004) 319–329.
- [3] H.N. Bhatti, A. Jabeen, M. Iqbal, S. Noreen, Z. Naseem, Adsorptive behavior of rice bran-based composites for malachite green dye: Isotherm, kinetic and thermodynamic studies, *J. Mol. Liq.*, 237 (2017) 322–333.
- [4] M. Salman, M. Athar, U. Farooq, Biosorption of heavy metals from aqueous solutions using indigenous and modified lignocellulosic materials, *Rev. Environ. Sci. Bio.*, 14 (2015) 211–228.
- [5] J.Y. Song, W.H. Zou, Y.Y. Bian, F.Y. Su, R.P. Han, Adsorption characteristics of methylene blue by peanut husk in batch and column modes, *Desalination*, 265 (2011) 119–125.
- [6] Y. Liu, X. Zhao, J. Li, D. Ma, R. Han, Characterization of biochar from pyrolysis of wheat straw and its evaluation on methylene blue adsorption, *Desal. Water Treat.*, 46 (2012) 115–123.
- [7] J.S. Mattson, H.B. Mark, Activated carbon: surface chemistry and adsorption from solution, M. Dekker 1971.
- [8] N. Jaafarzadeh, B. Kakavandi, A. Takdastan, R.R. Kalantary, M. Azizib, S. Jorfiab, Powder activated carbon/ Fe_3O_4 hybrid composite as a highly efficient heterogeneous catalyst for Fenton oxidation of tetracycline: Degradation mechanism and kinetic, *Rsc. Adv.*, 5 (2015) 84718–84728.
- [9] Y.K. Li, Y.D. Wang, Y. Zhang, R.P. Han, Y.Q. Li, Adsorption of 4-chlorophenol onto activated carbon prepared from wheat straw: equilibrium study, *Appl. Mech. Mater.*, 319 (2013) 245–248.
- [10] L.H. Ai, H.Y. Huang, Z.L. Chen, X. Wei, J. Jiang, Activated carbon/ $\text{Co Fe}_3\text{O}_4$ composites: Facile synthesis, magnetic performance and their potential application for the removal of malachite green from water, *Chem. Eng. J.*, 156 (2010) 243–249.
- [11] Y. Xu, J.J. Jin, X.L. Li, C.S. Song, H. Meng, X. Zhang, Adsorption behavior of methylene blue on Fe_3O_4 -embedded hybrid magnetic metal-organic framework, *Desal. Water. Treat.*, 57 (2016) 25216–25225.
- [12] H.R. Rajabi, H. Arjmand, S.J. Hoseini, H. Nasrabadi, Surface modified magnetic nano particles as efficient and green sorbents: Synthesis, characterization, and application for the removal of anionic dye, *J. Magn. Magn. Mater.*, 394 (2015) 7–13.
- [13] L.C.A. Oliveira, R. Rios, J.D. Fabris, K. Sapag, V.K. Garg, R.M. Lago, Clay-iron oxide magnetic composites for the adsorption of contaminants in water, *Appl. Clay. Sci.*, 22 (2003) 169–177.
- [14] M. Bhaumik, K. Setshedi, A. Maity, M.S. Onyango, Chromium (VI) removal from water using fixed bed column of polypyrrole/ Fe_3O_4 nano composite, *Sep. Purif. Technol.*, 110 (2013) 11–19.
- [15] J.W. Fu, Z.H. Chen, M.H. Wang, S.J. Liu, J.H. Zhang, J.N. Zhang, R.P. Han, Q. Xu, Adsorption of methylene blue by a high-efficiency adsorbent (polydopamine micro spheres): Kinetics, isotherm, thermodynamics and mechanism analysis, *Chem. Eng. J.*, 259 (2015) 53–61.
- [16] J.H. Wang, Y.F. Ji, S.L. Ding, H.R. Ma, X.J. Han, Adsorption and Desorption Behavior of Tannic Acid in Aqueous Solution on Polyaniline Adsorbent, *Chin. J. Chem. Eng.*, 21 (2013) 594–599.
- [17] S. Singh, Removal of Malachite green dye from Aqueous solution using Magnetic Activated Carbon, *Res. J. Chem. Sci.*, 6 (2015) 361–370.

- [18] S. Hamidzadeh, M. Torabbeigi, S.J. Shahataheri, Removal of crystal violet from water by magnetically modified activated carbon and nano magnetic iron oxide, *J. Environ. Health. Sci.*, 13 (2015) 1–7.
- [19] I. Savva, O. Marinica, C.A. Papatryfonos, L. Vekas, T. Krasia-Christoforou, Evaluation of electrospun polymer-Fe₃O₄ nano composite mats in malachite green adsorption, *Rsc. Adv.*, 5 (2015) 16484–16496.
- [20] L. Sun, S.C. Hu, H.M. Sun, H.L. Guo, H.D. Zhu, M.X. Liu, H.H. Sun, Malachite green adsorption onto Fe₃O₄@SiO₂-NH₂: isotherms, kinetic and process optimization, *Rsc. Adv.*, 5 (2015) 11837–11844.
- [21] S. Han, F. Zhao, J. Sun, B. Wang, R.Y. Wei, S.Q. Yan, Removal of p-nitrophenol from aqueous solution by magnetically modified activated carbon, *J. Magn. Mater.*, 341 (2013) 133–137.
- [22] N. Yang, S.M. Zhu, D. Zhang, S. Xu, Synthesis and properties of magnetic Fe₃O₄-activated carbon nano composite particles for dye removal, *Mater. Lett.*, 62 (2008) 645–647.
- [23] F. Jiang, D.M. Dinh, Y.-L. Hsieh, Adsorption and desorption of cationic malachite green dye on cellulose nano fibril aerogels, *Carbohydr. Polym.*, 173 (2017) 286–294.
- [24] D. Robati, M. Rajabi, O. Moradi, F. Najafi, I. Tyagi, S. Agarwal, V.K. Gupta, Kinetics and thermodynamics of malachite green dye adsorption from aqueous solutions on graphene oxide and reduced graphene oxide, *J. Mol. Liq.*, 214 (2016) 259–263.
- [25] M. Ghasemi, S. Mashhadi, M. Asif, I. Tyagi, S. Agarwal, V.K. Gupta, Microwave-assisted synthesis of tetraethylenepentamine functionalized activated carbon with high adsorption capacity for Malachite green dye, *J. Mol. Liq.*, 213 (2016) 317–325.
- [26] A. Mittal, Adsorption kinetics of removal of a toxic dye, Malachite Green, from wastewater by using hen feathers, *J. Hazard. Mater.*, 133 (2006) 196–202.
- [27] S. Nethaji, A. Sivasamy, G. Thennarasu, S. Saravanan, Adsorption of Malachite Green dye onto activated carbon derived from *Borassus aethiopicum* flower biomass, *J. Hazard. Mater.*, 181 (2010) 271–280.
- [28] A.S. Sartape, A.M. Mandhare, V.V. Jadhav, P.D. Raut, M.A. Anuse, S.S. Kolekar, Removal of malachite green dye from aqueous solution with adsorption technique using *Limonia acidissima* (wood apple) shell as low cost adsorbent, *Arab. J. Chem.*, 10 (2017) S3229–S3238.
- [29] Z.L. Wu, F. Liu, C.K. Li, X.Q. Chen, J.G. Yu, A sandwich-structured graphene-based composite: preparation, characterization, and its adsorption behaviors for Congo red, *Colloids Surf. A.*, 509 (2016) 65–72.
- [30] H.R. Rajabi, O. Khani, M. Shamsipur, V. Vatanpour, High-performance pure and Fe³⁺ ion doped ZnS quantum dots as green nano photo catalysts for the removal of malachite green under UV-light irradiation, *J. Hazard. Mater.*, 250–251 (2013) 370–378.
- [31] S.D. Khattri, M.K. Singh, Removal of malachite green from dye wastewater using neem sawdust by adsorption, *J. Hazard. Mater.*, 167 (2009) 1089–1094.
- [32] R. Malik, D.S. Ramteke, S.R. Wate, Adsorption of malachite green on groundnut shell waste based powdered activated carbon, *Waste Manage. (Oxford)*, 27 (2007) 1129–1138.
- [33] J.Y. Yang, X.Y. Jiang, F.P. Jiao, J.G. Yu, The oxygen-rich pentaerythritol modified multi-walled carbon nano tube as an efficient adsorbent for aqueous removal of alizarin yellow R and alizarin red S, *Appl. Surf. Sci.*, 436 (2018) 198–206.
- [34] J.G. Yu, J. Zou, L.L. Liu, X.Y. Jiang, F.P. Jiao, X.Q. Chen, J.G. Yu, J. Zou, L.L. Liu, X.Y. Jiang, Preparation of TiO₂-based photo catalysts and their photo catalytic degradation properties for methylene blue, rhodamine B and methyl orange, *Desalin. Water. Treat.*, 81 (2017) 282–290.
- [35] H.P. Boehm, Some aspects of the surface chemistry of carbon blacks and other carbons, *Carbon*, 32 (1994) 759–769.
- [36] I.K. Battisha, H.H. Afify, M. Ibrahim, Synthesis of Fe₂O₃ concentrations and sintering temperature on FTIR and magnetic susceptibility measured from 4 to 300 K of monolith silica gel prepared by sol-gel technique, *J. Magn. Mater.*, 306 (2006) 211–217.
- [37] V. Ranjithkumar, S. Sangeetha, S. Vairam, Synthesis of magnetic activated carbon/ α -Fe₂O₃ nano composite and its application in the removal of acid yellow 17 dye from water, *J. Hazard. Mater.*, 273 (2014) 127–135.
- [38] E. Atkins, Elements of X-ray Diffraction, *Phys. Today*, 10 (1978) 50–50.
- [39] L.C.A. Oliveira, R. Rios, J.D. Fabris, V. Garg, K. Sapag, R.M. Lago, Activated carbon/iron oxide magnetic composites for the adsorption of contaminants in water, *Carbon*, 40 (2002) 2177–2183.
- [40] R.D. Zhang, J.H. Zhang, X.N. Zhang, C.C. Dou, R.P. Han, Adsorption of Congo red from aqueous solutions using cationic surfactant modified wheat straw in batch mode: Kinetic and equilibrium study, *J. Taiwan Inst. Chem. E.*, 45 (2014) 2578–2583.
- [41] S. Chowdhury, R. Mishra, P. Saha, P. Kushwaha, Adsorption thermodynamics, kinetics and isosteric heat of adsorption of malachite green onto chemically modified rice husk, *Desalination*, 265 (2011) 159–168.
- [42] S.E. O'Reilly, D.G. Strawn, D.L. Sparks, Residence Time Effects on Arsenate Adsorption/Desorption Mechanisms on Goethite, *SSSAJ*, 65 (2001) 67–77.
- [43] S.K. Srivastava, R. Tyagi, Competitive adsorption of substituted phenols by activated carbon developed from the fertilizer waste slurry, *Water Res.*, 29 (1995) 483–488.
- [44] V.K. Garg, R. Kumar, R. Gupta, Removal of malachite green dye from aqueous solution by adsorption using agro-industry waste: a case study of *Prosopis cineraria*, *Dyes. Pigments*, 62 (2004) 1–10.
- [45] I.D. Mall, V.C. Srivastava, N.K. Agarwal, I.M. Mishra, Adsorptive removal of malachite green dye from aqueous solution by bagasse fly ash and activated carbon-kinetic study and equilibrium isotherm analyses, *Colloid. Surface. A.*, 264 (2005) 17–28.
- [46] S. Coruh, S. Elevli, Optimization of malachite green dye removal by sepiolite clay using a central composite design, *Global Nest J.*, 16 (2014) 340–348.
- [47] D.X. Wang, L.L. Liu, X.Y. Jiang, J.G. Yu, X.Q. Chen, Adsorption and removal of malachite green from aqueous solution using magnetic beta-cyclodextrin-graphene oxide nano composites as adsorbents, *Colloid. Surface. A.*, 466 (2015) 166–173.
- [48] M. Yu, Y.Y. Han, J. Li, L.J. Wang, CO₂-activated porous carbon derived from cattail biomass for removal of malachite green dye and application as super capacitors, *Chem. Eng. J.*, 317 (2017) 493–502.
- [49] F. Zhang, Z. Wei, W.N. Zhang, H. Cui, Effective adsorption of malachite green using magnetic barium phosphate composite from aqueous solution, *Spectrochim. Acta, Pt. A: Mol. Biomol. Spectrosc.*, 182 (2017) 116–122.
- [50] K. Porkodi, K.V. Kumar, Equilibrium, kinetics and mechanism modeling and simulation of basic and acid dyes sorption onto jute fiber carbon: Eosin yellow, malachite green and crystal violet single component systems, *J. Hazard. Mater.*, 143 (2007) 311–327.
- [51] S. Agarwal, I. Tyagi, V.K. Gupta, S. Mashhadi, M. Ghasemi, Kinetics and thermodynamics of Malachite Green dye removal from aqueous phase using iron nano particles loaded on ash, *J. Mol. Liq.*, 223 (2016) 1340–1347.
- [52] K. Gupta, O.P. Khatri, Reduced graphene oxide as an effective adsorbent for removal of malachite green dye: Plausible adsorption pathways, *J. Colloid Interface Sci.*, 501 (2017) 11–21.
- [53] Y.C. Lee, E.J. Kim, J.W. Yang, H.J. Shin, Removal of malachite green by adsorption and precipitation using aminopropyl functionalized magnesium phyllosilicate, *J. Hazard. Mater.*, 192 (2011) 62–70.
- [54] R.P. Han, Y. Wang, Q. Sun, L.L. Wang, J.Y. Song, X.T. He, C.C. Dou, Malachite green adsorption onto natural zeolite and reuse by microwave irradiation, *J. Hazard. Mater.*, 175 (2010) 1056–1061.
- [55] M.A. Ahmad, R. Alrozi, Removal of malachite green dye from aqueous solution using rambutan peel-based activated carbon: Equilibrium, kinetic and thermodynamic studies, *Chem. Eng. J.*, 171 (2011) 510–516.

- [56] G.S. Dawood, Removal Orange (G) Dye from aqueous solution by adsorption on bentonite, *Tikrit J. Pur. Sci.*, 15 (2010) 231–234.
- [57] C.H. Weng, Y.T. Lin, T.W. Tzeng, Removal of methylene blue from aqueous solution by adsorption onto pineapple leaf powder, *J. Hazard. Mater.* 170 (2009) 417–424.
- [58] T. Zhou, W.Z. Lu, L.F. Liu, H.M. Zhu, Y.B. Jiao, S.S. Zhang, R.P. Han, Effective adsorption of light green anionic dye from solution by CPB modified peanut in column mode, *J. Mol. Liq.*, 211 (2015) 909–914.
- [59] S. Sadaf, H.N. Bhatti, Evaluation of peanut husk as a novel, low cost biosorbent for the removal of Indosol Orange RSN dye from aqueous solutions: batch and fixed bed studies, *Clean Technol. Environ.*, 16 (2014) 527–544.
- [60] Y.B. Jiao, D.L. Han, Y.Z. Lu, Y.C. Rong, L.Y. Fang, Y.L. Liu, R.P. Han, Characterization of pine-sawdust pyrolytic char activated by phosphoric acid through microwave irradiation and adsorption property toward CDNB in batch mode, *Desal. Water. Treat.*, 77 (2017) 247–255.
- [61] R.P. Han, L.N. Zou, X. Zhao, Y.F. Xu, F. Xu, Y.L. Li, Y. Wang, Characterization and properties of iron oxide-coated zeolite as adsorbent for removal of copper (II) from solution in fixed bed column, *Chem. Eng. J.*, 149 (2009) 123–131.